Published in final edited form as:
Cell. 2014 June 5; 157(6): 1430–1444. doi:10.1016/j.cell.2014.05.015.

Subunit architecture and functional modular rearrangements of the transcriptional Mediator complex

Kuang-Lei Tsai[1], **Chieri Tomomori-Sato**[2], **Shigeo Sato**[2], **Ronald C. Conaway**[2,3], **Joan W. Conaway**[2,3], and **Francisco J. Asturias**[1]

[1]Department of Integrative Structural and Computational Biology, The Scripps Research Institute, La Jolla, CA 92037, USA

[2]Stowers Institute for Medical Research, Kansas City, MO 64110, USA

[3]Department of Biochemistry & Molecular Biology, Kansas University Medical Center, Kansas City, KS 66160, USA

SUMMARY

The multisubunit Mediator comprising ~30 distinct proteins, plays an essential role in gene expression regulation by acting as a bridge between DNA binding transcription factors and the RNA polymerase II (RNAPII) transcription machinery. Efforts to uncover the Mediator mechanism have been hindered by a poor understanding of its structure, subunit organization, and conformational rearrangements. By overcoming biochemical and image analysis hurdles, we obtained accurate EM structures of yeast and human Mediators. Subunit localization experiments, docking of partial X-ray structures, and biochemical analyses resulted in comprehensive mapping of yeast Mediator subunits and a complete reinterpretation of our previous Mediator organization model. Large-scale Mediator rearrangements depend on changes at the interfaces between previously described Mediator modules, which appear to be facilitated by factors conducive to transcription initiation. Conservation across eukaryotes of Mediator structure, subunit organization, and RNA polymerase II interaction suggest conservation of fundamental aspects of the Mediator mechanism.

Correspondence should be addressed to: F.J.A. (asturias@scripps.edu).

ACCESSION NUMBERS

EM maps of yeast and human Mediators were deposited to the EMDataBank with accession numbers EMD-2634 (yeast) and EMD-2635 (human).

SUPPLEMENTARY INFORMATION

Supplementary information includes Extended Experimental Procedures, 6 figures, one table, one movie, and a Supplementary Dataset.

AUTHOR CONTRIBUTIONS

All experiments, except those dealing with human Mediator purification and subunit interactions, were designed by K-L. T. and F.A., and carried out by K-L. T. K-L. T. and F.A. discussed and interpreted yeast Mediator results and wrote the manuscript with help from R.C.C., and J.W.C. Human Mediator purification and subunit interaction experiments were designed, discussed, and interpreted by C.T.-S., S.S., R.C.C., and J.W.C. and carried out by C.T.-S. and S.S.

INTRODUCTION

Mediator, a large complex comprising 25–30 different proteins with a combined mass in excess of 1MDa, plays an essential role in transcriptional regulation in all eukaryotes (Malik and Roeder, 2010). Mediator subunits are organized into 3 core modules (Head, Middle, and Tail), which are devoid of enzymatic activity, and a dissociable CDK8 kinase module (CKM). Components of each module are thought to be structurally and functionally connected (Figure 1A).

Despite its critical importance, the detailed molecular mechanisms by which Mediator affects transcription are poorly understood. Mediator can physically interact with a collection of transcriptional regulatory proteins, including DNA binding transcription factors, RNA polymerase II (RNAPII), general initiation factors, and transcription elongation factors. As a consequence of these interactions, Mediator can regulate RNAPII at both the initiation and elongation stages of transcription (Conaway and Conaway, 2013; Malik and Roeder, 2010).

A long-standing model, supported by various studies (Cai et al., 2009; Davis et al., 2002; Ebmeier and Taatjes, 2010; Taatjes et al., 2002; Taatjes et al., 2004), is that Mediator's ability to transmit signals from DNA binding transcription factors to RNAPII might be based on modulation of Mediator's conformation. For example, interaction of Mediator with RNAPII requires a considerable reorganization of the Mediator structure that is favored in Mediator bound to transcriptional factors (Bernecky et al., 2011; Davis et al., 2002).

Understanding the mechanisms by which Mediator regulates transcription will require an understanding of its subunit organization, conformational behavior, and interactions. However, because of its size and complexity, Mediator represents a daunting challenge for high-resolution structural analysis by X-ray crystallography. To date, the largest Mediator subcomplex characterized at high resolution is the yeast Head module (Imasaki et al., 2011; Lariviere et al., 2012; Robinson et al., 2012), which includes 7 Mediator proteins. In addition, a number of structures of single subunits or subunit segments are available (Baumli et al., 2005; Hoeppner et al., 2005; Koschubs et al., 2009; Lariviere et al., 2006; Vojnic et al., 2011), and a model of the *S. cerevisiae* Middle module based on partial X-ray structures of component subunits and data from protein crosslinking and mass spectrometry data was published recently (Lariviere et al., 2013).

Static structures of Mediator subcomplexes are not sufficient to reveal how the complete Mediator complex controls transcription. Structures of full Mediator complexes and information about conformational changes have come from single particle electron microscopy (EM) studies (Asturias et al., 1999; Cai et al., 2009; Naar et al., 2002; Taatjes et al., 2002), but until now, the quality and interpretation of these EM structures have been limited by the problems associated with analysis of Mediator samples displaying considerable heterogeneity in conformation and/or composition. As importantly, information about subunit localization essential to interpret the Mediator structures, conformational changes, and interactions, has been extremely sparse.

Here we present a molecular map detailing the location and interactions of all 25 yeast Mediator (yMED) proteins. Optimization of specimen preparation and image analysis protocols allowed us to finally obtain a homogeneous enough yMED preparation and an accurate EM map of the complex. Furthermore, the use of EM image analysis approaches specifically designed to address the challenges associated with characterization of less homogeneous samples allowed us to determine the location of all yMED proteins, which guided docking of published X-ray structures of yMED components into our EM map of the complex. We followed similar approaches to calculate an accurate map of human Mediator (hMED), which includes a number of subunits not found in yMED, and we arrived at a partial description of hMED subunit organization, including localization of the critical metazoan-specific subunit MED26. Our results reveal a remarkable degree of conservation of the Mediator structure and subunit organization across eukaryotes. Leveraging the value of our EM Mediator maps by docking of partial high-resolution structures allowed us to identify and describe subunit interfaces that facilitate rearrangements of the Mediator structure, to define subunits contributing to interaction with RNAPII, and to propose a model for how specific factors might affect Mediator conformation. Taken together, our observations support a model for how modulation of conserved Mediator structure and interactions might make a fundamental contribution to the Mediator mechanism for regulation of transcription initiation.

RESULTS

Cryo-EM structure of yMED

We purified yMED using a modified version of an immunoaffinity protocol we developed for a previous EM study of yMED (Cai et al., 2009). Success of the cryo-EM analysis was critically dependent on obtaining a yMED preparation that was as homogeneous as possible. We screened a number of different yMED constructs by both SDS-PAGE and EM and selected as the best one with a Protein A/maltose-binding protein (MBP) tag at the Med16 C-terminus and a calmodulin-binding-peptide tag at the Med5 N-terminus. We prepared EM samples and recorded approximately 85,000 images of yMED particles preserved in amorphous ice (Figure S1A). These yMED cryo-EM images were computationally screened and clustered. Most of the resulting image class averages corresponded to different projections of core yMED devoid of the CKM (Figure S1B).

To validate an initial low resolution yMED structure, we calculated 2 maps independently and using different approaches (see Extended Experimental Procedures and Figure S1C–D). Correspondence between these maps (Figure S1E) established the validity our initial yMED structure to a resolution of 3.5–4.0 nm. Further map refinement resulted in a yMED cryo-EM map with a resolution of ~1.8 nm (Figure S1F–H). Comparing the present cryo-EM map to our previous one (Figure S1I) (Cai et al., 2009) showed a similar overall shape and dimensions, but considerable differences in detail. The increased quality of our present yMED cryo-EM map was due to optimization of the yMED preparation and the use of EM image analysis protocols specifically tailored to address challenges associated with yMED conformational variability. Some residual variability in yMED conformation apparent in yMED class averages (Figure S1B) was addressed by sorting yMED cryo-images into 5

groups and calculating corresponding 3D maps that showed similar features in slightly different relative arrangements (Figure S1J). For all further analysis we used the yMED map corresponding to class I (Figures 1B and S1J).

Localization and mapping of yMED subunits and modules

The large number of Mediator components, combined with the limited quality and resolution of available EM maps of the complex, have prevented localization of Mediator subunits through docking of high-resolution structures. Nonetheless, localizing individual Mediator proteins is essential to establish the molecular organization of the complex, interpret biochemical and functional data, and, ultimately, determine Mediator mechanism. Therefore, we pursued Mediator subunit localization by EM imaging of particles in which the position of an individual protein was pinpointed either (i) through labeling with antibodies directed against engineered tags), (ii) through introduction of a large "marker" (e.g., maltose-binding protein; MBP) engineered into the protein in question, (iii) through deletion of one or more protein components, or (iv) through sub-complex purification. We used SDS-PAGE analysis to ensure that labeling or deletion of specific subunits did not compromise the integrity of yMED in any way that could obscure interpretation of the subunit localization results (Figure S2).

Localization of the Head module and its subunits—We had previously proposed that the Head module might correspond to one end of the Mediator structure based, not on direct subunit localization results, but on analysis of 2D images of a Tail-less holoenzyme complex (Dotson et al., 2000). When the Head's X-ray structure was determined a decade later (Imasaki et al., 2011), its overall size and shape seemed to be compatible with what we believed at the time to be the Head portion of the best available yMED cryo-EM map (Cai et al., 2009). However, the reliability of the comparison between the X-ray and EM maps was greatly limited by the low resolution of the EM structure. To unequivocally determine the position of the Head module we decided to focus on localization of 3 Head subunits, Med8, Med18 and Med20. Med18 and Med20 form the self-contained movable jaw portion of the Head's structure (Figure 2A), which connects to the rest of the Head through the Med8 C-terminus (Lariviere et al., 2006); thus we surmised that deletion of the movable jaw or labeling of the Med8 C-term would result in minimal disruption of the Mediator complex. We localized the Med8 C-terminus through an engineered MBP tag, and localized Med18-Med20 by deleting Med18, which resulted in loss of Med18 and Med20 density (Med20 associates through Med18 and is lost when Med18 is deleted; Figure S2B). To our surprise, all 3 subunits were localized in a small region half-way between the top and bottom of the Mediator structure (Figures 2B and S3A–B). This, combined with unequivocal docking of the X-ray structure of the Head (Robinson et al., 2012) made possible by improved accuracy and resolution of our yMED cryo-EM map, resulted in definitive localization of the module (Figure 2C). The conformation of the Head appears to be constrained by contacts with other portions of the Mediator complex because, although an isolated recombinant Head module can undergo dramatic conformational changes (Cai et al., 2010), the conformation of the Head in the context of the entire Mediator closely matches that observed in the X-ray structures. Therefore, docking of the Head's X-ray structure established the position of all other Head module subunits not directly localized by EM experiments. The largest contact

between the Head and the rest of Mediator involves an extensive surface that is located on one face of the Head's fixed jaw and is largely formed by Med17. This explains why the Head module is easily lost in the *srb4-138* temperature-sensitive mutant allele in which a number of point mutations destabilize the fixed jaw (Linder et al., 2006). Smaller contacts are established through an area around the patch of the Head's neck where the RNAPII CTD binds (Robinson et al., 2012), and through the tips of the Head jaws (Figure 2C). Further analysis of the subunit organization of yMED revealed the identity of the interacting partners of these Head module regions.

Localization of the Middle module and its subunits—We localized 7 out of 8 subunits in the Middle module through deletion of individual subunits (Med1, Med9, Med19, Med31), and/or through C-terminal MBP labeling (Med7, Med9, Med10, Med21, and Med31) (Figures 2D–E and S3A–B). EM analysis of a Med19Δ Med7-TAP mutant Mediator revealed nearly intact Mediator particles in which only the "hook" at the top of the Mediator structure was missing, identifying the Med19 location. Deletion of Med1 also resulted in nearly intact Mediator particles in which only the globular density to the left of the Mediator structure was absent. Deletion of Med9 gave a similar result, suggesting that Med9 is located near Med1. C-terminal MBP labeling of Med9 and 4 additional Middle module subunits (Med7, Med10, Med21, and Med31) localized their C-termini to the portion of the yMED structure spanning the distance between Med19 and Med1. We found a nice correspondence in the position of subunits localized through both labeling and deletion (Med9 and Med31). This established that the Middle module starts at the hook near the top of the yMED structure and extends downwards toward Med1 (Figures 2D–E).

Further analysis of the Med19Δ Med7-TAP images provided interesting additional information and confirmed that the Middle module has an elongated structure with Med19 and Med1 at either end. Besides particles missing only Med19 (the hook), two additional types of particles were present in the Med19Δ EM samples. One corresponded to a Mediator subcomplex in which Med19, Med1, and the entire density between them was missing. The second type was elongated particles matching the size and shape of the portion of the yMED structure from Med1 to the Med10 location (Figure S3D). Our EM observations are in agreement with results from a biochemical study of Med19Δ yMED, which also identified the same 3 types of complexes (Med19Δ Mediator, Mediator without a Middle module, and Med19Δ Middle module) and was the first report of a direct Head-Tail interaction in Mediator (Baidoobonso et al., 2007). The information from our Middle module subunit localization studies is also in full agreement with a recent X-ray model of a Middle module subcomplex that includes all Middle subunits except Med1 and Med19 and is based on partial X-ray structures and cross-linking/mass spectrometry analysis (Lariviere et al., 2013). Docking of this model, guided by our Middle module subunit localization results, shows that it corresponds closely to the structure of the Middle module portion of our yMED cryo-EM map (Figure 2F). A conserved hinge that allows the Med7-Med21 complex to adopt different conformations (Baumli et al., 2005) is located right at the base of the Med19 hook, and might explain the exceptionally high mobility of that portion of the yMED structure. Although a large fraction of the 25 kDa Med19 subunit is peripherally located on the hook, Med19 is clearly critical for stable interaction of the Middle module with Mediator. This

effect of Med19 on Mediator stability might come about indirectly through contacts between Med19 and other Middle module subunits, including possible extension of Med19 beyond the hook.

Docking of the Middle module X-ray model into our yMED cryo-EM map also reveals that interaction of the Middle module with the Head depends on the Med7 N-terminus (Med7N) and Med31 subunits. Localization of Med31 was especially important because the subunit is highly conserved and the Med31-Med7N subcomplex forms a protrusion in the Middle module model that could be used to confirm correct docking into the yMED cryo-EM map. Hence, we verified the location of Med31 through both deletion of the subunit and MBP labeling of its C-terminus (Figures 2D–E and S3A–B). Med31 is located right across the CTD-binding patch on the Head's neck (Figure 2F), and labeling or deletion of Med31 disrupts its interaction with the Head's neck, as we describe below.

Localization of the Tail module and its subunits—We localized Tail subunit Med5 (129 kDa) through deletion and also through antibody labeling of its N-terminus. Deletion of Med5 resulted in loss of density at the tip of the bottom domain in the yMED structure and antibody labeling localized Med5 to the same area (Figures 2G and S3B). We also pursued localization of Med16 (111 kDa) through MBP labeling of its C-terminus, which was mapped to an area around the connection between the bottom domain containing Med5 and the rest of the Mediator structure (Figures 2G and S3A). This result alone was insufficient to localize Med16, but we found that introducing a TAP-tag at the C-terminus of a truncated Med16 (Med16 aa 1-866) caused a Med5-Med16 subcomplex to separate from the rest of Mediator (Figure S3E). This allowed us to determine an EM map of the Med5-Med16 heterodimer (Figure 2G). Comparing this Med5-Med16 map to the corresponding portion of the yMED structure (as determined by the position of Med5) indicated that the large, self-contained bottom domain of the yMED structure, with a volume corresponding to ~400 kDa) is mostly formed by Med5 and Med16. The distal position of the Med5 N-terminus is consistent with reported interaction of Med5 with the rest of Mediator through Med16 (Beve et al., 2005).

Consistent with a reported role of Med16 in stabilizing interaction of other Tail subunits with yMED (Li et al., 1995), the connection from the bottom domain to the rest of yMED was not apparent in the map of the Med5-Med16 subcomplex determined from the Med16 C-terminal truncation strain. To learn more about the organization of the connection between the Med5-Med16 heterodimer and the rest of Mediator we pursued localization of additional Tail module subunits by C-terminal MBP tagging. We found that the C-termini of Med2, Med3, and Med15 are located around the connection (Figures 2H and S3A). It has been reported that Med2-Med3-Med15 can form a stable subcomplex (Beve et al., 2005; Zhang et al., 2004) and we were able to purify such a subcomplex from a yeast strain with a TAP-tag on Med2 and a C-terminal Med16 truncation (Med16 aa 1-551) (Figure S3F). Images of the Med2-Med3-Med15 heterotrimer matched the size and shape of the elbow-shaped connection between Med5-Med16 and the rest of Mediator, indicating that Med2, Med3, and Med15 form that part of the yMED structure (Figures 2H). The Med2-Med3-Med15 particles imaged by EM appear somewhat small to account for the combined mass of all 3 proteins (48, 43, and 120 kDa, respectively), suggesting that a portion of the

subcomplex could be disordered, perhaps due to disruption of contacts with Med5-Med16. In fact, EM analysis of yMED particles purified from a Med15Δ strain generated a 2D map that matched exactly the top portion of the yMED structure, but lacked the Med5-Med16 domain and its connection (Figure S3G), indicating that most or all of Med15 must be part of the bottom domain and its connection to the rest of the yMED structure.

Also consistent with an early observation that C-terminal truncation of Med14 caused loss of Tail module subunits (Li et al., 1995), MBP tagging of the Med14 C-terminus localized it at the corner of the Med2-Med3-Med15 connector to the Med5-Med16 domain (Figures 2G and S3A). Therefore, the Med14 and Med16 C-termini are located at opposite ends of the Med2-Med3-Med15 connector, offering a clue for how they might play a critical role in stabilizing integration of Tail subunits into Mediator.

Taken together, the results just described indicate that 5 out of 6 Tail module subunits (Med2, Med3, Med5, Med15, and Med16) form the bottom domain and its connection to the top portion of the yMED structure (Figure 2I), leaving outstanding only localization of Med14, one of the largest yMED proteins (123 kDa). We localized the Med14 C-terminus to the distal end of the bottom yMED domain that contains most Tail subunits, but concluded that the majority of Med14 density could not be located within that portion of the yMED structure. Therefore, we pursued localization of the Med14 N-terminus by antibody labeling of an engineered 3xHA tag and found it to be near the center of the yMED structure (Figure 2H). Hence, the Med14 N- and C-termini are located at opposite ends of a relatively large density in the top portion of the yMED structure, which remained unaccounted for after fitting of the Head and Middle X-ray structures. That Med14 forms this large, central “core” interface connecting the Head module’s fixed jaw, the central portion of the Middle module, and the bottom domain formed by other Tail subunits was confirmed by considering results from EM and SDS-PAGE analysis of Med15Δ yMED. As indicated, class averages calculated from Med15Δ yMED images (Figure S3G) show an intact top portion of the yMED structure. The SDS-PAGE results show that deletion of Med15 leads to loss of all Tail module subunits, except Med14, which remains associated with the Head and Middle modules (Figure S2B). In conclusion, all of these observation, together with fitting of the Head and Middle module X-ray structures show that Med14 forms a “core” interface that contacts components from all 3 yMED modules (Figure 2I). Consistent with this central location, Med14 has not been traditionally considered as a Tail component, but rather as a Middle module protein that is important for interfacing with the Tail (Li et al., 1995).

In summary, we were able to use direct experimental results and published information about Mediator structure and organization from various sources to localize all subunits in core yMED, define yMED module boundaries (Figure 3A), and characterize module interfaces and the subunits that form them. These results represent a complete revision of our previous understanding of yMED module organization, which was based only on indirect information and limited by the comparatively low quality of previous yMED EM maps. Our present conclusions are based on multiple, internally-consistent results, and provide a complete, definitive, and reasonably precise description of yMED’s subunit architecture. As suggested by biochemical studies, the Head, Middle, and Tail modules form self-contained segments of the Mediator structure connected by relatively small interfaces

(Figure 3A). Our previous work on the dissociable CDK8 kinase module (CKM) (Tsai et al., 2013) completes mapping of all 25 subunits in yeast Mediator. The CKM interacts with core Mediator primarily through a contact between its Med13 subunit and Med19 in the Middle module, and through contacts between the Cdk8 kinase and the portion of the Head module connecting the Head's neck to the area around the Med18-Med20 movable Head jaw (Figure 3B).

hMED 3D structure and conservation of Mediator's overall architecture

To compare the structures of the yeast and human Mediators we pursued EM characterization of hMED immunopurified from HeLa cells. As was the case with yMED, the choice of the tagged subunit used for purification was essential to obtain an hMED preparation suitable for EM analysis and we obtained the most homogeneous preparations by purifying hMED through a FLAG tag engineered into the N-terminus of the metazoan-specific specific subunit MED26 (Figure S2C).

MED26 is associated with a fraction of human Mediator that is largely free of CKM (Mittler et al., 2001; Paoletti et al., 2006; Sato et al., 2004; Taatjes, 2010) and appears to play a key role in transcriptional activation (Mo et al., 2004; Naar et al., 2002; Ryu et al., 1999; Takahashi et al., 2011). We recorded images of hMED particles after particle preservation in stain and used them to calculate 2D image class averages corresponding to various hMED views (Figure 4A). Although MED26-containing hMED represents only a fraction of total hMED (Paoletti et al., 2006), 2D class averages of MED26-hMED appear indistinguishable from averages we calculated earlier from images of hMED purified through a nuclear receptor bound to Med1 (Tsai et al., 2013). We obtained an initial low resolution hMED map (see Extended Experimental Procedures and Figure S4A) and used it as the starting point for calculating an hMED map with a resolution of ~3.0 nm (Figures 4B and S4B–C).

The refined yMED and hMED maps show a similar overall organization, with portions of the hMED map resembling in shape and position the yMED Head, Middle, and Tail, modules (Figure 4C). The Head and Middle modules showed more than an overall resemblance, as evidenced by docking of the X-ray structure of the yeast Head module and the yeast Middle module model into the hMED map (Figure S4D). As in yMED, most of the hMED Tail module density sits below the Head and Middle modules, but the human Tail module is larger, and the connectivity between the hMED Tail and the Head and Middle modules differs, with a clear connection between the end of the Middle module corresponding to yMED's Med1 and the Tail, and a much larger interface between hMED's Tail and the Head jaws (Figure 4C).

The overall structure of Mediator appears to be largely conserved from yeast to humans. The similarity in shape and relative arrangement of the Head and Middle modules is particularly striking and suggests that their organization could be conserved between yeast and human Mediators. Our biochemical analyses of human Mediator support the conclusion that this is indeed the case. By assessing the ability of epitope-tagged human Mediator subunits transiently overexpressed in HEK293T cells to associate with one another, we generated an interaction map of evolutionarily conserved and metazoan-specific human Mediator subunits. These analyses produced several notable findings. First, conserved human Head

module subunits MED6, MED8, MED11, MED17, MED18, MED20, and MED22 engage in an extensive network of interactions with one another, as is observed in the X-ray structure of the yeast Head module (Imasaki et al., 2011; Lariviere et al., 2012; Robinson et al., 2012) (Figures 5A and S5A). Second, our results argue that the evolutionarily conserved human Middle module subunits MED1, MED4, MED7, MED9, MED10, MED21, and MED31 interact with one another through a network (Figures 5B and S5B) very similar to that proposed for the yeast Middle module subunits (Hallberg et al., 2006; Koschubs et al., 2010; Lariviere et al., 2013) and detected by our EM analysis of yMED (Figure 2D–F). Third, our findings are consistent with localization of human MED19 near the Head-Middle interface, just as we observed for yeast Med19 through labeling and deletion EM studies. In particular, we detected strong MED19 interactions with conserved Middle module subunit MED31 (Figures 5C) and with Head module subunits MED6 and MED8. In yMED, the “hook” formed by Med19 is immediately adjacent to Med31 and the N-termini of Med6 and Med8. Thus, not only are the structures of the yeast and human Head and Middle modules conserved, but so are at least some key aspects of their mode of interaction. Fourth, analyses of the hMED Tail module (Figure S5C) showed that conserved Tail subunits MED14, MED15, and MED16 interact with subunits MED23 and MED24, which have previously been assigned to the hMED Tail module based on evidence that loss of either one leads to disruption of the Tail and to loss of Med16 (Ito et al., 2002; Stevens et al., 2002). Our results also strongly support the idea that the metazoan-specific subunit MED25, which engages in an extensive network of interactions with other Tail proteins, must be a component of the Tail module. We note that MED24 has been proposed to be a metazoan ortholog of yeast Med5 (Bourbon, 2008). If that were the case, one would expect MED15, MED23, and MED25 to bridge MED16 and MED24 to other hMED subunits.

Our biochemical and EM experiments also provided insights into how some metazoan-specific subunits associate with hMED. In reciprocal co-immunoprecipitation assays we detected a strong interaction between MED26 and MED19 (Figure 5C). We also obtained evidence that MED26 associates with the Middle module via interactions with MED4 and MED7, as both subunits (especially MED7), were immunoprecipitated with anti-FLAG antibodies when co-expressed with FLAG-MED26 (Figure 5D). To correlate these biochemical observations to structural data, we pursued localization of FLAG-MED26 by recording EM images of FLAG-MED26 hMED (the same preparation used for calculation of the hMED EM map) after labeling with anti-FLAG antibodies. Interpretation of these EM images was complicated by apparent high mobility of the FLAG-tagged MED26 N-terminus. Therefore, we instead analyzed hMED containing a conserved N-terminally FLAG-tagged MED26 C-terminal domain (Figure S2C) (residues 421-600; FLAG-MED26C) that is sufficient for assembly into Mediator (Takahashi et al., 2011). These experiments localized MED26 to a structure homologous to the hook formed by Med19 in yMED and in close proximity to the positions occupied by yMED’s Med4 and the Med7 N-term (Figure S4E). Mediator can be isolated from human cells in two major forms that contain either MED26 or the CKM. For this reason, we speculated that MED26 and the CKM might be in dynamic equilibrium with the Mediator core and that it might be possible to exchange exogenously added MED26 for MED26 associated with hMED. Consistent with this possibility, we found that after incubation of FLAG-MED26 hMED with

recombinant GST-MED26, additional density was again found on the hook and in close proximity to the positions occupied by yMED's Med4 and the Med7 N-term (Figure S4F and 5E).

Notably, the MED26-MED4-MED7 interaction was substantially increased when MED21 was also present (Figure 5D). We obtained no biochemical evidence for direct binding of MED21 to MED26, but in yMED Med21 is near the area corresponding to the location of MED26 in hMED. Tight association between Mediator subunits indicated by our subunit tagging and deletion studies in yMED (disruption of a subunit often results in reduced overall complex stability), and by the highly interconnected structure of the yMED Head module (Imasaki et al., 2011; Lariviere et al., 2012; Robinson et al., 2012), could help explain how MED21 might contribute to stabilization of MED26 interaction with neighboring hMED subunits. These observations bolster the proposition that subunit organization is conserved between yMED and hMED.

We also observed that the metazoan-specific subunits MED27, MED28, MED29, and MED30 make extensive contacts both with evolutionarily conserved Head module subunits and with each other (Figure 5A). Two observations suggest that MED29 and perhaps other Head-associated metazoan-specific subunits could contribute to the additional density observed between the Head jaws and the Tail module in hMED. First, it was shown previously that MED29 interacts directly and strongly with subunit MED20 and indirectly with MED18 (Sato et al., 2003a), the subunits that form the movable Head jaw in yMED (Imasaki et al., 2011). Second, although still controversial, it has been proposed that MED29 could be a highly divergent ortholog of yeast Med2 (Bourbon, 2008), which in yMED is part of the elbow shaped connection between the Tail module and the Head jaws (Figures 2H and 3B). In the future, the same approaches used to localize MED26 can be applied to localization of other metazoan-specific hMED proteins and will eventually result in a complete map of hMED subunit organization.

Mediator rearrangements and structural interfaces

Several EM studies have suggested that conformational changes are an essential component of the Mediator mechanism (Davis et al., 2002; Meyer et al., 2010; Naar et al., 2002; Taatjes et al., 2002; Taatjes et al., 2004). However, an understanding of Mediator rearrangements, the way in which they come about and are controlled, and their effect on Mediator interactions, has remained elusive due to low reliability/resolution of the EM structures (likely caused by variability in particle composition and/or conformation) and a lack of information about subunit organization required to interpret them. Therefore, we decided to investigate structural rearrangements in yMED considering our new understanding of the subunit organization of the complex.

An isolated Head module can undergo significant rearrangements (Cai et al., 2012; Cai et al., 2010) and it has been suggested that the Middle modules could adopt different conformations as well (Baumli et al., 2005). However, we found that X-ray structures of the Head and Middle modules could be directly fitted into the yMED EM map (Figures 2C, 2F, and 3), indicating that the structures of the individual modules in the context of the entire Mediator are relatively stable. Thus, at least to a first approximation, changes in yMED

conformation come from changes in the relative position of its Head, Middle, and Tail modules, and not from changes in the structure of the modules themselves.

To investigate whether changes at the interfaces between modules might influence Mediator conformation, we focused on the subunits at the Head-Middle and Head-Tail module interfaces (Figure 6A). The Head-Middle interface is formed by a contact between the Head's neck and Med7-N/Med31 in the Middle module (Figure 6A). Variability in the position of the Head's neck was observed in ISAC averages of wild-type yMED particles preserved in ice (Figure S1B), suggesting that this could be a dynamic module interface. In fact, we found that MBP labeling of the Med31 C-terminus, or deletion of Med31, resulted in 2D averages in which the Head's neck is no longer attached to the Middle module, indicative of a disrupted interaction with the Head's neck that results in increased Head mobility (Figure 6B).

The Head-Tail interface is very extensive (Figure 6A). There is a large contact formed mainly by Med17 in the Head's fixed jaw and the centrally located Med14. This interface must be relatively stable because in image class averages where deletion of Med19 results in loss of the entire Middle module, the Head and Tail modules can still form a complex in which the modules adopt the same relative orientation as in wt yMED (Figure 6B). At the same time, the interface is capable of large rearrangements without major disruption of its Head or Tail module components, because the Head can swing away under various conditions, leaving behind well-defined Med14 density (Figure 6B). When the Head swings away from Med14, it remains connected through a second Head-Tail contact formed by the tips of the Head jaws and the Med2-Med3-Med15 connector to the bottom portion of the Tail (Med5-Med16). Deletion of Med18 (and concomitant loss of Med20) results in expected loss of the Head's movable jaw (Figure 2B), but, if the Head's connections to the Middle module and Med14 are lost, can also result in complete repositioning of the Head, with the Head again swinging outwards and away from the rest of Mediator (Figure 6B). This suggests that both Head jaws are involved in interaction with Tail subunits in yMED, and likely also in hMED (Sato et al., 2003a). Direct interaction of the Head's movable jaw (formed by Med18 and Med20) with the Med2-Med3-Med15 connection would be consistent with reported targeting of Med2, Med3, Med15, and Med20 by the Gcn4 (Zhang et al., 2004), Gal4 (Reeves and Hahn, 2005), Cha4 (Kim and Gross, 2013), Pdr1 (Ansari et al., 2012), and Oaf1 (Thakur et al., 2009) activators, and involvement of these subunits in RNAPII and TBP recruitment to a promoter (Zhang et al., 2004).

In conclusion, the results from our EM analysis of the yMED structure and the way in which it is affected by labeling or deletion of specific subunits, support the idea that the structure of individual yMED modules is fairly stable, and that module interfaces play an essential role in facilitating conformational changes in Mediator.

Mediator conformation and RNAPII interaction

To investigate the possible functional significance of yMED conformational rearrangements facilitated by changes at inter-module contacts, we decided to compare them to yMED rearrangements to the ones observed in the yMED-RNAPII-TFIIF holoenzyme. To this end, we used our new understanding of the yMED structure to re-interpret a 3D EM map of the

yMED-RNAPII-TFIIF holoenzyme (Davis et al., 2002) calculated from images of holoenzyme particles purified from yeast (Kim et al., 1994). We started by segmenting our new yMED cryo-EM map into its component modules (Figure 6C, left) with the Tail module divided into the bottom Med5-Med16 portion (in yellow) and the Med2-Med3-Med15/Med14 connection to the Head and Middle (in gray). In the published yMED-RNAPII-TFIIF holoenzyme map, RNAPII appears as a compact, globular density making well-defined contacts with Mediator. This, and our improved understanding of the yMED structure allowed us to identify density corresponding to yMED and fit the Head, Middle, and Tail module segments of our new yMED cryo-EM map into the Mediator portion of the published holoenzyme map.

Distinguishing features of all 3 Mediator modules, such as the jaws and neck sections of the Head module, the Med19 hook at the top of the Middle module, the Med5-Med16 section of the Tail module, the elbow-shaped Med2-Med3-Med15 connection between the Head jaws and the Med5-Med16 section of the Tail, could be easily recognized in the holoenzyme structure from Davis et al. Rigid docking of the modules from our new yMED cryo-EM map into the holoenzyme map accounted for all Mediator density and provided a very revealing depiction of the changes in yMED conformation required for interaction with RNAPII (Figure 6C).

When yMED forms part of the holoenzyme, the Head and Middle modules undergo a coordinated rotation of ~80°. In addition, a rearrangement of the Med2-Med3-Med15/Med14 connector results in rotation of the Tail module by ~30° (Animation S1). This analysis conclusively establishes that large conformational rearrangements of the yMED structure required for interaction with RNAPII are made possible by changes at module interfaces, and brings up the question of how changes at these interfaces might be controlled. To investigate the possible effect of transcription factors on yMED module interfaces and overall yMED conformation, we examined the effect of the RNAPII CTD and the Gcn4 activator on yMED conformation.

Binding of the RNAPII CTD to a patch on the Head's neck domain (Robinson et al., 2012) initiates what appears to be a multi-step process of yMED-RNAPII holoenzyme formation (Tsai et al., 2013). Our subunit localization results show that in yMED, the Head's neck domain contacts a portion of the Middle module formed by Med7N-Med31 (Figure 6A). The X-ray structure of Med7N-Med31 revealed that 2 segments of the Med7 N-term bear a resemblance to the heptapeptide sequence repeats in the CTD (Koschubs et al., 2009), raising the possibility that CTD binding might disrupt interaction of the Head's neck with Med7N-Med31 and facilitate a rearrangement of the yMED structure. We therefore analyzed the conformation of yMED particles after incubation with a recombinant GST-labeled CTD. We could detect GST-CTD density in only ~10% of single yMED images, but comparing averages obtained through clustering of yMED images before and after incubation with the CTD revealed a marked increase in the conformational variability of yMED particles caused by CTD interaction (Figures 6D and S6A), suggesting a dynamic CTD-yMED interaction that can have a persistent effect on yMED conformation.

After incubation with the recombinant GST-CTD, some yMED averages show the standard conformation (Figure S6B, framed in green). However, other averages show the Middle module swinging out (Figure S6B, framed in yellow), and a third group of averages shows a coordinated rotation of the Middle and Head modules (Figure S6B, framed in red), evidenced by lengthening of the projection of the elongated Med1 subunit at the bottom end of the Middle module and disappearance of the characteristic “double hump” created by the projection of the Head’s neck and movable jaw. These are precisely the same changes in yMED conformation observed upon formation of the yMED-RNAPII-TFIIF holoenzyme (Figure 6C). Interestingly, the same motions are occasionally observed in yMED alone, but incubation with the CTD results in a much larger proportion of yMED particles showing repositioning of the Middle and Head modules. Whereas ~70% of yMED particles alone show the “standard conformation”, only ~35% of yMED particles show the standard conformation after incubation with the GST-CTD. The other 65% of particles show repositioning of the Middle and/or Head modules due to either a shift in the position of the Middle module (~50%), or coordinated rotation of the Middle and Head modules (~15%) (Figure 6D). CTD-induced changes in hMED conformation were reported before (Naar et al., 2002), but their nature or significance could not be explained at the time.

We also evaluated the effect on yMED conformation of interaction with the yeast Gcn4 activator by re-analyzing yMED images recorded in an earlier study to monitor changes in RNAPII position after incubation with Gcn4 (Tsai et al., 2013). By focusing on yMED conformation instead of RNAPII position we found that, consistent with reported “fuzzy” binding of Gcn4 to Med15 (Brzovic et al., 2011), no clear Gcn4 density was detected, but interaction with the activator caused a rearrangement of the Med2-Med3-Med15 connector and rotation of the Tail module in ~20% of yMED particles (Figure 6E, compare to projection view of the holoenzyme in Figures 6C). This rearrangement is either entirely absent or too rare for detection in yMED alone.

In summary, we obtained information about possible structural rearrangements of yMED from 4 independent sources: docking of yMED modules into a previously reported EM map of the yMED-RNAPII-TFIIF holoenzyme (Figure 6C and Animation S1), analysis of conformational variability in yMED particles (Figure S6A), analysis of conformational variability in yMED particles after incubation with a GST-CTD (Figures 6D and S6), and analysis of conformational changes in yMED particles after incubation with the Gcn4 activator (Figure 6E). These different analyses provide a consistent description of Mediator conformational changes: structural interfaces between Mediator modules make possible rearrangements that prepare Mediator for interaction with RNAPII by moving the Middle module away from the space eventually occupied by RNAPII, rotating the Head module, and repositioning the Tail module.

DISCUSSION

Optimization of biochemical and image analysis protocols allowed us to overcome the challenge posed by compositional and conformational variability of yeast Mediator and calculate a reliable and accurate EM map of the complex. Although the resolution is still somewhat limited by conformational variability, the improved accuracy of the new yMED

map and our new EM subunit localization results allowed us to dock the X-ray structures of the Head and Middle modules and define the position of the 15 yMED subunits they include. Additional comprehensive subunit mapping results revealed the location of all Tail module subunits. Taken together with our previous work on the CDK8 kinase module (Tsai et al., 2013), our results now provide a complete molecular description of yMED's subunit organization, module boundaries, inter-module contacts, and subunit interactions (Figure 3).

We found that large-scale yMED conformational changes are facilitated by rearrangements at module interfaces (Figure 6C and Animation S1), and that these interfaces appear to be targeted by specific factors. Interaction of the CTD with the Head-Middle interface appears to destabilize the interface and facilitate a concerted rotation of the Middle and Head modules (Figures 6D and S6), and interaction of the Gcn4 activator with the Head-Tail interface appears to facilitate rotation of the Tail module (Figure 6E). A previous study (Naar et al., 2002) reported that CTD binding induced changes in hMED conformation and suggested that the changes were similar to changes induced by interaction with the VP-16 activator. However, the nature of those changes could not be interpreted in the absence of any information about module or subunit organization in human Mediator. Consideration of the changes in yMED structure we have observed, together with the yMED organization apparent in yMED-RNAPII-TFIIF holoenzyme particles purified directly from yeast (Davis et al., 2002), suggests that interaction with the CTD and Gcn4 could push the yMED conformation closer to that observed in the holoenzyme. Movement of the Middle module out of the site occupied by RNAPII in holoenzyme particles, repositioning of the Head so that the Head jaws directly face the RNAPII site, and rotation of the Tail, would presumably facilitate the specific mode of Mediator-RNAPII interaction observed in the holoenzyme. Like Gcn4, many other activators target Med2, Med3, and/or Med15 (Ansari et al., 2012; Kim and Gross, 2013; Reeves and Hahn, 2005; Zhang et al., 2004) and could have similar effects on yMED conformation. Comprehensive functional studies beyond the scope of the present work, such as mutational analyses and activity assays, will be required to explore these issues further and establish possible functional consequences of the Mediator rearrangements we have observed.

The dramatic difference between the initial CTD-dependent position for RNAPII interaction with yMED (Tsai et al., 2013) (Figure 7A) and the position that RNAPII occupies in the yMED-RNAPII-TFIIF holoenzyme (Davis et al., 2002) (Figure 6C), suggests that establishment of a fully functional Mediator-RNAPII complex might involve multiple steps (Tsai et al., 2013) (Figure 7B) and that the structure of the Mediator-RNAPII-TFIIF holoenzyme we analyzed could differ in important ways from that of a fully-formed initiation complex. Consistent with this idea, although the preponderant Mediator-RNAPII arrangement in the yMED-RNAPII-TFIIF holoenzyme we analyzed is one in which Rpb3 and Med17 are juxtaposed and interaction between these subunits has been reported to be functionally significant *in vivo* (Soutourina et al., 2011), the orientation of RNAPII in the holoenzyme particles is variable (Tsai et al., 2013). Involvement of the general transcription factors and other components of the transcription apparatus, including activators and promoter DNA, is likely to be essential for full and consequential interaction of Mediator and RNAPII, as proposed for hMED (Bernecky et al., 2011). The results we report here

suggest that modulation of yMED conformation could be critical for controlling yMED-RNAPII interaction.

In conclusion, our results, combined with those of others, point to an important "mechanical" aspect to the Mediator regulatory mechanism, consistent with the lack of enzymatic activity in core Mediator. Our map of human Mediator, in which we identify structural modules very similar to those in yMED, provides strong evidence that overall Mediator architecture is conserved across eukaryotes. In addition, class averages calculated from images of hMED-RNAPII complexes present in our hMED samples immunopurified through tagged MED26 show that binding of polymerase to human Mediator happens at a location corresponding to the one observed for CTD-dependent RNAPII binding to yMED (Tsai et al., 2013) (Figure 7A). The structure of a published 3D EM map of a hMED-TFIIF-RNAPII complex prepared in the presence of the VP16 activator (Bernecky et al., 2011) suggests that the RNAPII position in that complex might correspond to that occupied by RNAPII in the yMED-RNAPII-TFIIF holoenzyme. Conservation of fundamental Mediator architecture and RNAPII interaction suggest conservation across eukaryotes of these mechanical components of the mechanism by which Mediator regulates transcription. Conceivably, the capacity of Mediator to integrate signals from various regulatory factors that impinge on regulation of a promoter could be at least partially explained by the cooperative effect of various factors targeting different Mediator interfaces, but all leading to a Mediator rearrangement required for consequential interaction with RNAPII. In this scenario, the increased complexity of Mediator in higher organisms could be explained by increased complexity of inter-module contacts enabled by the presence of metazoan-specific subunits.

EXPERIMENTAL PROCEDURES

A detailed description of all experimental procedures is provided in Supplementary Extended Experimental Procedures.

Yeast Strains

A PCR-based genomic epitope-tagging method was used to construct strains with various affinity tags in different subunits starting with the protease-deficient yeast strain BJ2168 (ATCC, 208277). For subunit deletions or truncations, a PCR-amplified kanMX6 cassette from plasmid pFA6a-kanMX6 (Bahler et al., 1998) was used to replace either a specific region, or the entirety of an open reading frame. All yeast strains used in this study are listed in Table S1.

Yeast Mediator Purification

All of the Mediator used in our studies were purified essentially as described before (Tsai et al., 2013). All purified protein complexes were characterized by SDS-PAGE analysis and EM to monitor their quality prior to use for EM data collection. See Extended Experimental Procedures for further details.

Human Mediator purification

hMED was purified from HeLa-S3 cells stably expressing either FLAG-MED26 or FLAG-C-MED26. Nuclear extracts were prepared from ~2.5×10^{10} cells as described (Abmayr et al., 2006).

Biochemical analysis of mammalian Mediator subunit interactions

Interactions between exogenously expressed human or mouse MED subunits were performed essentially as described (Sato et al., 2003b).

Electron Microscopy and Image Processing

Stained specimens of yeast and human Mediators were preserved with 0.75% (w/v) uranyl formate. Cryo-EM yMED specimens were prepared on perforated carbon grids covered with a continuous amorphous carbon film and vitrified in liquid ethane. EM images were automatically acquired with Leginon (Suloway et al., 2005) and recorded on a K2 Summit direct electron detector (Gatan, Inc.) operating in counting mode. All image analysis was carried out using the SPARX EM image processing package (Hohn et al., 2007). EM map interpretation, docking of the X-ray structures, and image rendering were carried out using the UCSF-Chimera software package (Pettersen et al., 2004).

Supplementary Material

Refer to Web version on PubMed Central for supplementary material.

Acknowledgments

This work was supported by US National Institutes of Health grants R01 GM67167 (F.J.A.) and R01 GM41628 (R.C.C. and J.W.C) and by a grant to the Stowers Institute from the Helen Nelson Medical Research Fund at the Greater Kansas City Community Foundation. We thank Y. Takagi for providing the plasmid for MBP-tagging in yeast, G.C. Lander for critical reading of manuscript, and thank Patrick Cramer for providing a Med19Δ yeast strain. EM data collection was carried out at the National Resource for Automated Macromolecular Microscopy (NRAMM).

References

Abmayr SM, Yao T, Parmely T, Workman JL. Preparation of nuclear and cytoplasmic extracts from mammalian cells. Curr Protoc Mol Biol. 2006; Chapter 12(Unit 12):11.

Ansari SA, Ganapathi M, Benschop JJ, Holstege FC, Wade JT, Morse RH. Distinct role of Mediator tail module in regulation of SAGA-dependent, TATA-containing genes in yeast. EMBO J. 2012; 31:44–57. [PubMed: 21971086]

Asturias FJ, Jiang YW, Myers LC, Gustafsson CM, Kornberg RD. Conserved structures of mediator and RNA polymerase II holoenzyme. Science. 1999; 283:985–987. [PubMed: 9974391]

Bahler J, Wu JQ, Longtine MS, Shah NG, McKenzie A 3rd, Steever AB, Wach A, Philippsen P, Pringle JR. Heterologous modules for efficient and versatile PCR-based gene targeting in Schizosaccharomyces pombe. Yeast. 1998; 14:943–951. [PubMed: 9717240]

Baidoobonso SM, Guidi BW, Myers LC. Med19(Rox3) regulates Intermodule interactions in the Saccharomyces cerevisiae mediator complex. J Biol Chem. 2007; 282:5551–5559. [PubMed: 17192271]

Baumli S, Hoeppner S, Cramer P. A conserved mediator hinge revealed in the structure of the MED7.MED21 (Med7.Srb7) heterodimer. J Biol Chem. 2005; 280:18171–18178. [PubMed: 15710619]

Bernecky C, Grob P, Ebmeier CC, Nogales E, Taatjes DJ. Molecular architecture of the human Mediator-RNA polymerase II-TFIIF assembly. PLoS Biol. 2011; 9:e1000603. [PubMed: 21468301]

Beve J, Hu GZ, Myers LC, Balciunas D, Werngren O, Hultenby K, Wibom R, Ronne H, Gustafsson CM. The structural and functional role of Med5 in the yeast Mediator tail module. J Biol Chem. 2005; 280:41366–41372. [PubMed: 16230344]

Bourbon HM. Comparative genomics supports a deep evolutionary origin for the large, four-module transcriptional mediator complex. Nucleic Acids Res. 2008; 36:3993–4008. [PubMed: 18515835]

Brzovic PS, Heikaus CC, Kisselev L, Vernon R, Herbig E, Pacheco D, Warfield L, Littlefield P, Baker D, Klevit RE, et al. The acidic transcription activator Gcn4 binds the mediator subunit Gal11/Med15 using a simple protein interface forming a fuzzy complex. Mol Cell. 2011; 44:942–953. [PubMed: 22195967]

Cai G, Chaban YL, Imasaki T, Kovacs JA, Calero G, Penczek PA, Takagi Y, Asturias FJ. Interaction of the Mediator Head Module with RNA Polymerase II. Structure. 2012; 20:899–910. [PubMed: 22579255]

Cai G, Imasaki T, Takagi Y, Asturias FJ. Mediator structural conservation and implications for the regulation mechanism. Structure. 2009; 17:559–567. [PubMed: 19368889]

Cai G, Imasaki T, Yamada K, Cardelli F, Takagi Y, Asturias FJ. Mediator head module structure and functional interactions. Nat Struct Mol Biol. 2010; 17:273–279. [PubMed: 20154708]

Conaway RC, Conaway JW. The Mediator complex and transcription elongation. Biochimica et biophysica acta. 2013; 1829:69–75. [PubMed: 22983086]

Davis JA, Takagi Y, Kornberg RD, Asturias FA. Structure of the yeast RNA polymerase II holoenzyme: Mediator conformation and polymerase interaction. Mol Cell. 2002; 10:409–415. [PubMed: 12191485]

Dotson MR, Yuan CX, Roeder RG, Myers LC, Gustafsson CM, Jiang YW, Li Y, Kornberg RD, Asturias FJ. Structural organization of yeast and mammalian mediator complexes. Proc Natl Acad Sci. 2000; 97:14307–14310. [PubMed: 11114191]

Ebmeier CC, Taatjes DJ. Activator-Mediator binding regulates Mediator-cofactor interactions. Proc Natl Acad Sci U S A. 2010; 107:11283–11288. [PubMed: 20534441]

Ge K, Cho YW, Guo H, Hong TB, Guermah M, Ito M, Yu H, Kalkum M, Roeder RG. Alternative mechanisms by which mediator subunit MED1/TRAP220 regulates peroxisome proliferator-activated receptor gamma-stimulated adipogenesis and target gene expression. Mol Cell Biol. 2008; 28:1081–1091. [PubMed: 18039840]

Hallberg M, Hu GZ, Tronnersjo S, Shaikhibrahim Z, Balciunas D, Bjorklund S, Ronne H. Functional and physical interactions within the middle domain of the yeast mediator. Mol Genet Genomics. 2006; 276:197–210. [PubMed: 16758199]

Hoeppner S, Baumli S, Cramer P. Structure of the mediator subunit cyclin C and its implications for CDK8 function. J Mol Biol. 2005; 350:833–842. [PubMed: 15979093]

Hohn M, Tang G, Goodyear G, Baldwin PR, Huang Z, Penczek PA, Yang C, Glaeser RM, Adams PD, Ludtke SJ. SPARX, a new environment for Cryo-EM image processing. J Struct Biol. 2007; 157:47–55. [PubMed: 16931051]

Imasaki T, Calero G, Cai G, Tsai KL, Yamada K, Cardelli F, Erdjument-Bromage H, Tempst P, Berger I, Kornberg GL, et al. Architecture of the Mediator head module. Nature. 2011; 475:240–243. [PubMed: 21725323]

Ito M, Okano HJ, Darnell RB, Roeder RG. The TRAP100 component of the TRAP/Mediator complex is essential in broad transcriptional events and development. EMBO J. 2002; 21:3464–3475. [PubMed: 12093747]

Kim S, Gross DS. Mediator recruitment to heat shock genes requires dual Hsf1 activation domains and mediator tail subunits Med15 and Med16. J Biol Chem. 2013; 288:12197–12213. [PubMed: 23447536]

Kim YJ, Bjorklund S, Li Y, Sayre MH, Kornberg RD. A multiprotein mediator of transcriptional activation and its interaction with the C-terminal repeat domain of RNA polymerase II. Cell. 1994; 77:599–608. [PubMed: 8187178]

Koschubs T, Lorenzen K, Baumli S, Sandstrom S, Heck AJ, Cramer P. Preparation and topology of the Mediator middle module. Nucleic Acids Res. 2010; 38:3186–3195. [PubMed: 20123732]

Koschubs T, Seizl M, Lariviere L, Kurth F, Baumli S, Martin DE, Cramer P. Identification, structure, and functional requirement of the Mediator submodule Med7N/31. Embo J. 2009; 28:69–80. [PubMed: 19057509]

Lariviere L, Geiger S, Hoeppner S, Rother S, Strasser K, Cramer P. Structure and TBP binding of the Mediator head subcomplex Med8-Med18-Med20. Nat Struct Mol Biol. 2006; 13:895–901. [PubMed: 16964259]

Lariviere L, Plaschka C, Seizl M, Petrotchenko EV, Wenzeck L, Borchers CH, Cramer P. Model of the Mediator middle module based on protein cross-linking. Nucleic Acids Res. 2013; 41:9266–9273. [PubMed: 23939621]

Lariviere L, Plaschka C, Seizl M, Wenzeck L, Kurth F, Cramer P. Structure of the Mediator head module. Nature. 2012; 492:448–451. [PubMed: 23123849]

Li Y, Bjorklund S, Jiang YW, Kim YJ, Lane WS, Stillman DJ, Kornberg RD. Yeast global transcriptional regulators Sin4 and Rgr1 are components of mediator complex/RNA polymerase II hologenzyme. Proc Natl Acad Sci USA. 1995; 92:10864–10868. [PubMed: 7479899]

Linder T, Zhu X, Baraznenok V, Gustafsson CM. The classical srb4–138 mutant allele causes dissociation of yeast Mediator. Biochem Biophys Res Commun. 2006; 349:948–953. [PubMed: 16962561]

Malik S, Roeder RG. The metazoan Mediator co-activator complex as an integrative hub for transcriptional regulation. Nat Rev Genet. 2010; 11:761–772. [PubMed: 20940737]

Meyer KD, Lin SC, Bernecky C, Gao Y, Taatjes DJ. p53 activates transcription by directing structural shifts in Mediator. Nat Struct Mol Biol. 2010; 17:753–760. [PubMed: 20453859]

Mittler G, Kremmer E, Timmers HT, Meisterernst M. Novel critical role of a human Mediator complex for basal RNA polymerase II transcription. EMBO reports. 2001; 2:808–813. [PubMed: 11559591]

Mo X, Kowenz-Leutz E, Xu H, Leutz A. Ras induces mediator complex exchange on C/EBP beta. Mol Cell. 2004; 13:241–250. [PubMed: 14759369]

Naar AM, Taatjes DJ, Zhai W, Nogales E, Tjian R. Human CRSP interacts with RNA polymerase II CTD and adopts a specific CTD-bound conformation. Genes Dev. 2002; 16:1339–1344. [PubMed: 12050112]

Paoletti AC, Parmely TJ, Tomomori-Sato C, Sato S, Zhu D, Conaway RC, Conaway JW, Florens L, Washburn MP. Quantitative proteomic analysis of distinct mammalian Mediator complexes using normalized spectral abundance factors. Proc Natl Acad Sci U S A. 2006; 103:18928–18933. [PubMed: 17138671]

Pettersen EF, Goddard TD, Huang CC, Couch GS, Greenblatt DM, Meng EC, Ferrin TE. UCSF Chimera--a visualization system for exploratory research and analysis. J Comput Chem. 2004; 25:1605–1612. [PubMed: 15264254]

Reeves WM, Hahn S. Targets of the Gal4 transcription activator in functional transcription complexes. Mol Cell Biol. 2005; 25:9092–9102. [PubMed: 16199885]

Robinson PJ, Bushnell DA, Trnka MJ, Burlingame AL, Kornberg RD. Structure of the Mediator Head module bound to the carboxy-terminal domain of RNA polymerase II. Proc Natl Acad Sci U S A. 2012; 109:17931–17935. [PubMed: 23071300]

Ryu S, Zhou S, Ladurner AG, Tjian R. The transcriptional cofactor complex CRSP is required for activity of the enhancer-binding protein Sp1. Nature. 1999; 397:446–450. [PubMed: 9989412]

Sato S, Tomomori-Sato C, Banks CA, Parmely TJ, Sorokina I, Brower CS, Conaway RC, Conaway JW. A mammalian homolog of Drosophila melanogaster transcriptional coactivator intersex is a subunit of the mammalian Mediator complex. J Biol Chem. 2003a; 278:49671–49674. [PubMed: 14576168]

Sato S, Tomomori-Sato C, Banks CA, Sorokina I, Parmely TJ, Kong SE, Jin J, Cai Y, Lane WS, Brower CS, et al. Identification of mammalian Mediator subunits with similarities to yeast Mediator subunits Srb5, Srb6, Med11, and Rox3. J Biol Chem. 2003b; 278:15123–15127. [PubMed: 12584197]

Sato S, Tomomori-Sato C, Parmely TJ, Florens L, Zybailov B, Swanson SK, Banks CA, Jin J, Cai Y, Washburn MP, et al. A set of consensus mammalian mediator subunits identified by

multidimensional protein identification technology. Mol Cell. 2004; 14:685–691. [PubMed: 15175163]

Soutourina J, Wydau S, Ambroise Y, Boschiero C, Werner M. Direct interaction of RNA polymerase II and mediator required for transcription in vivo. Science. 2011; 331:1451–1454. [PubMed: 21415355]

Stevens JL, Cantin GT, Wang G, Shevchenko A, Berk AJ. Transcription control by E1A and MAP kinase pathway via Sur2 mediator subunit. Science. 2002; 296:755–758. [PubMed: 11934987]

Suloway C, Pulokas J, Fellmann D, Cheng A, Guerra F, Quispe J, Stagg S, Potter CS, Carragher B. Automated molecular microscopy: the new Leginon system. J Struct Biol. 2005; 151:41–60. [PubMed: 15890530]

Taatjes DJ. The human Mediator complex: a versatile, genome-wide regulator of transcription. Trends Biochem Sci. 2010; 35:315–322. [PubMed: 20299225]

Taatjes DJ, Naar AM, Andel F 3rd, Nogales E, Tjian R. Structure, function, and activator-induced conformations of the CRSP coactivator. Science. 2002; 295:1058–1062. [PubMed: 11834832]

Taatjes DJ, Schneider-Poetsch T, Tjian R. Distinct conformational states of nuclear receptor-bound CRSP-Med complexes. Nat Struct Mol Biol. 2004; 11:664–671. [PubMed: 15195149]

Takahashi H, Parmely TJ, Sato S, Tomomori-Sato C, Banks CA, Kong SE, Szutorisz H, Swanson SK, Martin-Brown S, Washburn MP, et al. Human mediator subunit MED26 functions as a docking site for transcription elongation factors. Cell. 2011; 146:92–104. [PubMed: 21729782]

Thakur JK, Arthanari H, Yang F, Chau KH, Wagner G, Naar AM. Mediator subunit Gal11p/MED15 is required for fatty acid-dependent gene activation by yeast transcription factor Oaf1p. J Biol Chem. 2009; 284:4422–4428. [PubMed: 19056732]

Tsai KL, Sato S, Tomomori-Sato C, Conaway RC, Conaway JW, Asturias FJ. A conserved Mediator-CDK8 kinase module association regulates Mediator-RNA polymerase II interaction. Nat Struct Mol Biol. 2013; 20:611–619. [PubMed: 23563140]

Vojnic E, Mourao A, Seizl M, Simon B, Wenzeck L, Lariviere L, Baumli S, Baumgart K, Meisterernst M, Sattler M, et al. Structure and VP16 binding of the Mediator Med25 activator interaction domain. Nat Struct Mol Biol. 2011; 18:404–409. [PubMed: 21378965]

Zhang F, Sumibcay L, Hinnebusch AG, Swanson MJ. A triad of subunits from the Gal11/tail domain of Srb mediator is an in vivo target of transcriptional activator Gcn4p. Mol Cell Biol. 2004; 24:6871–6886. [PubMed: 15254252]

HIGHLIGHTS

- Mediator structure and molecular organization are conserved from yeast to humans
- Changes at Mediator module interfaces facilitate critical functional rearrangements
- Mediator conformation is directly influenced by factors conducive to transcription
- Pathway for polymerase interaction and basic Mediator mechanism are conserved

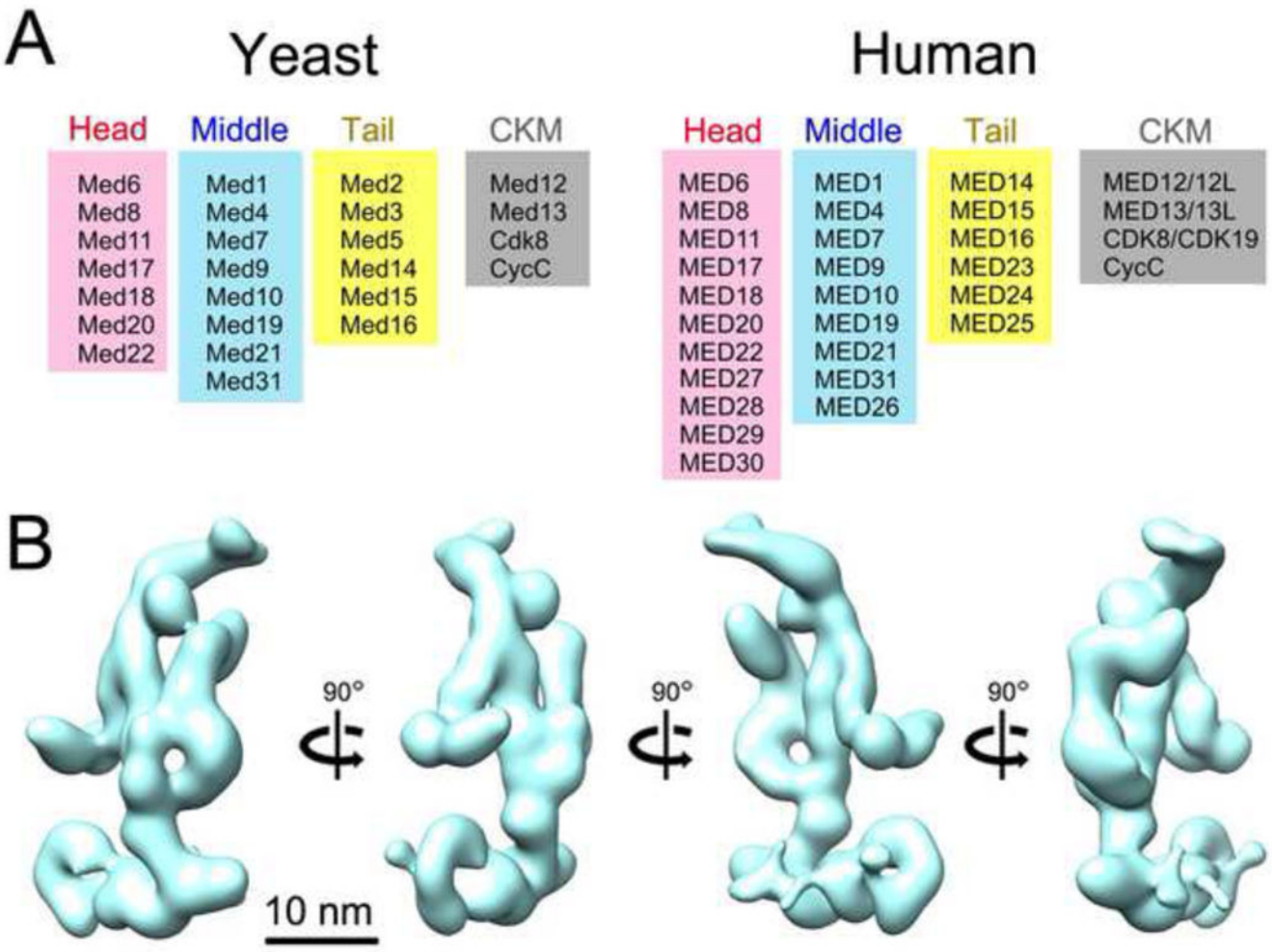

Figure 1. Mediator subunit organization, and structure of yMED

(A) Subunit organizations of yeast and human Mediators (25 and 30 different protein components, respectively). Biochemical and functional data indicates that Mediator subunits are organized into 4 different modules: Head, Middle, Tail, and a dissociable CDK8 kinase module (CKM).

(B) Various views of a 3D map of yMED calculated from images of single yMED particles preserved in amorphous ice. The resolution of the map is estimated at ~1.8 nm. See also Figure S1.

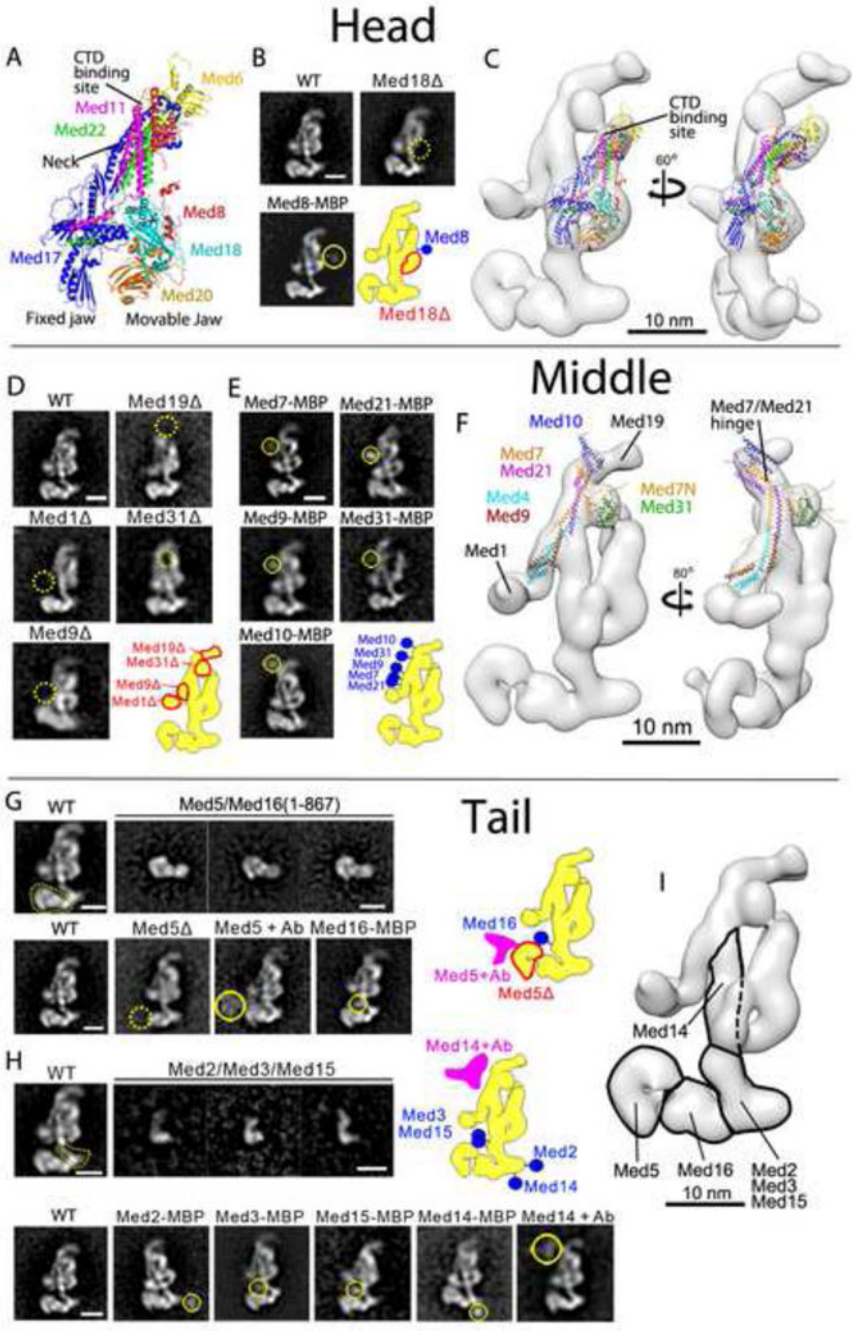

Figure 2. Localization of individual yMED subunits

(A) X-ray structure of the Head module. Head module proteins adopt a highly integrated structure, with the exception of Med18-Med20, which form the relatively independent movable jaw targeted in our subunit localization experiments.

(B) Localization of Head subunits through subunit deletion or C-terminal MBP tagging. Yellow circles superimposed on image class averages point to the position of an MBP tag at the Med8 C-term, and the area where density corresponding to Med18-Med20 is missing

after deletion of Med18. Changes evident in the class averages are schematized in the Mediator diagram.

(C) Docking of the Head's X-ray structure into the yMED cryo-EM map. The position of the patch where the RNAPII CTD binds is indicated.

(D) Localization of Middle module subunits through subunit deletion. Yellow circles superimposed on image class averages point to areas where density is missing after deletion of Med1, Med9, Med19, or Med31. Changes evident in the class averages are schematized in the Mediator diagram.

(E) Localization of Middle module subunits through C-terminal MBP tagging. Yellow circles superimposed on image class averages point to the positions of MBP tags at the Med7, Med9, Med10, Med21, and Med31 C-termini. Changes evident in the class averages are schematized in the Mediator diagram.

(F) Docking of a model of the Middle module, based on partial X-ray structures and crosslinking-mass spectrometry analysis, into the yMED cryo-EM map. The positions of all Middle module subunits, determined through direct subunit localization experiments and confirmed by docking of the X-ray model, are indicated.

(G) Image class averages showing the structure of a Med5-Med16 (1-866) subcomplex, and localization of Med5 and Med 16 through subunit deletion, MBP tagging, and antibody labeling. The structure of the Med5-Med16 (1-866) subcomplex matches the structure of a large portion of the yMED bottom domain. Yellow circles superimposed on image class averages point to areas where density is missing after deletion of Med5, or additional density is apparent after MBP tagging of Med5 or Med16, and after antibody labeling of the Med5 N-term. Changes evident in the class averages are schematized in the Mediator diagram.

(H) Image class averages showing the structure of a Med2-Med3-Med15 subcomplex, which matches that of the density connecting the top and bottom portions of the yMED structure. Also, localization of Med2, Med3, and Med 15 through C-terminal MBP tagging resulted in additional density highlighted by yellow circles superimposed on image class averages. C-terminal MBP tagging and N-terminal antibody of Med14 are also shown. Changes evident in the class averages are schematized in the Mediator diagram.

(I) A diagram indicating the location and density distribution of Tail module subunits. See also Figures S2 and S3, Supplemental Dataset 1, and Table S1.

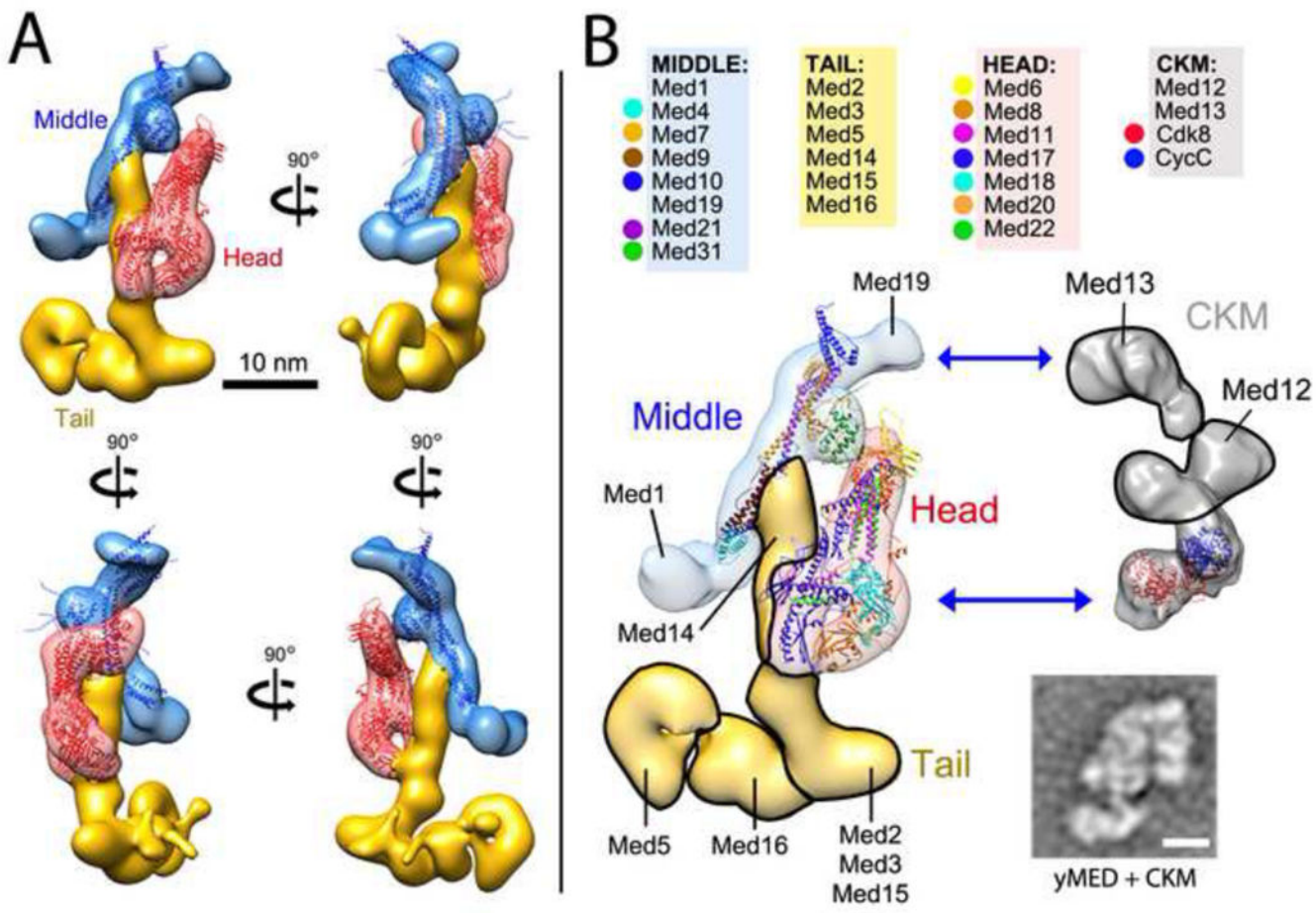

Figure 3. Modular and subunit organization of yMED

(A) Position, boundaries, and relative arrangement of the Head, Middle, and Tail yMED modules.

(B) Position and relative arrangement of all 25 yMED subunits (including those in the dissociable CKM module). Available X-ray structures are shown docked into the yMED cryo-EM map. The inset shows a class average calculated from images of yMED-CKM particles, illustrating the interaction between core yMED and the dissociable CKM subcomplex (Tsai et al., 2013). Scale bar corresponds to 10.0 nm. See also Figure S3.

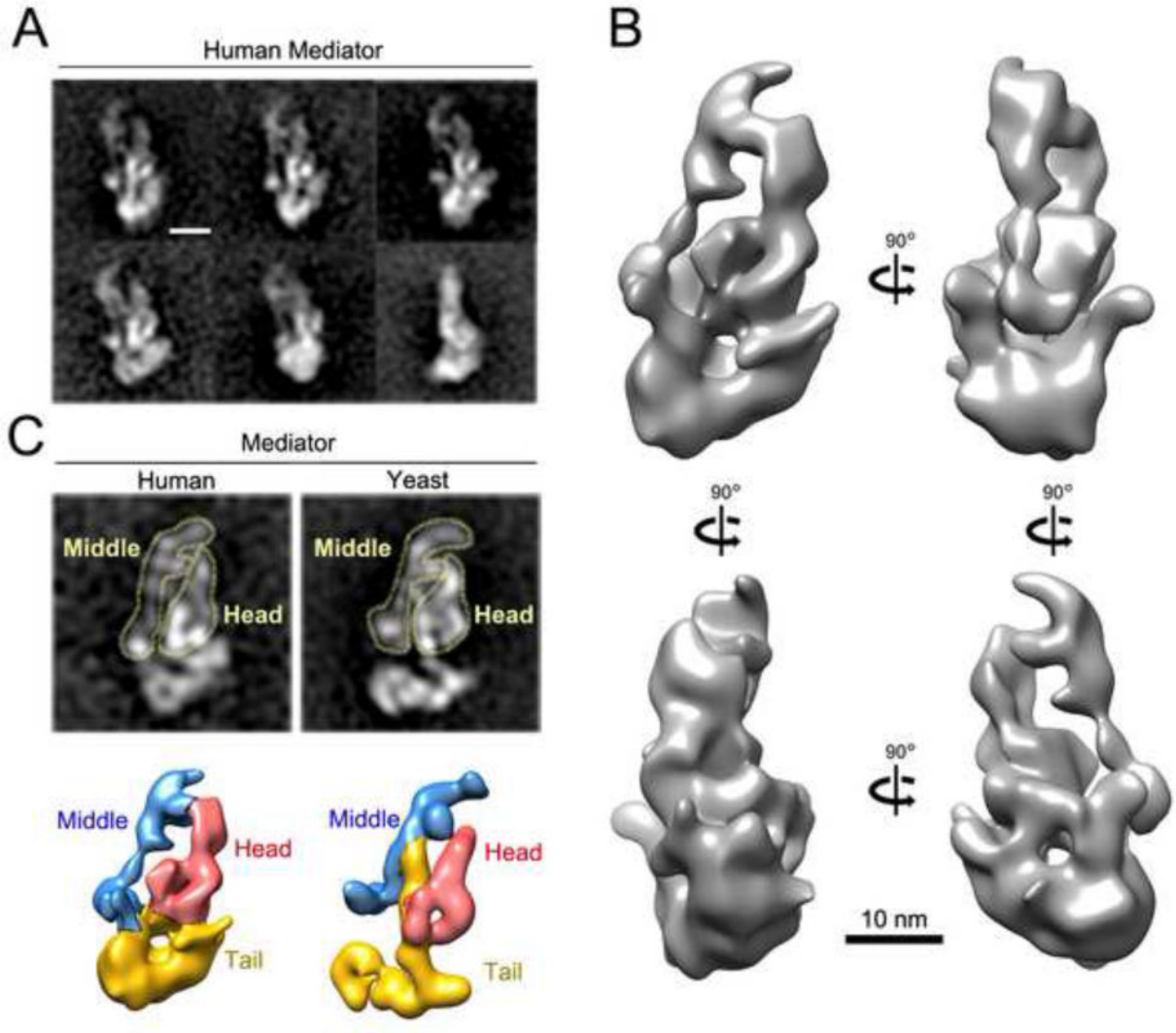

Figure 4. Structure and modular organization of hMED

(A) Class averages calculated from images of hMED particles preserved in stain show various views of the complex. Scale bar corresponds to 10.0 nm.

(B) EM map of hMED calculated from images of single hMED particles preserved in stain. The resolution of the map is estimated at ~3 nm. Scale bar corresponds to 10 nm.

(C) Comparing the structures of yeast and human Mediator highlights a correspondence between them and can be used to tentatively identify modules and module boundaries in hMED. The overall structure and interactions of the Head, Middle, and Tail modules, appear to be conserved between yeast and human Mediators. See also Figure S4D.

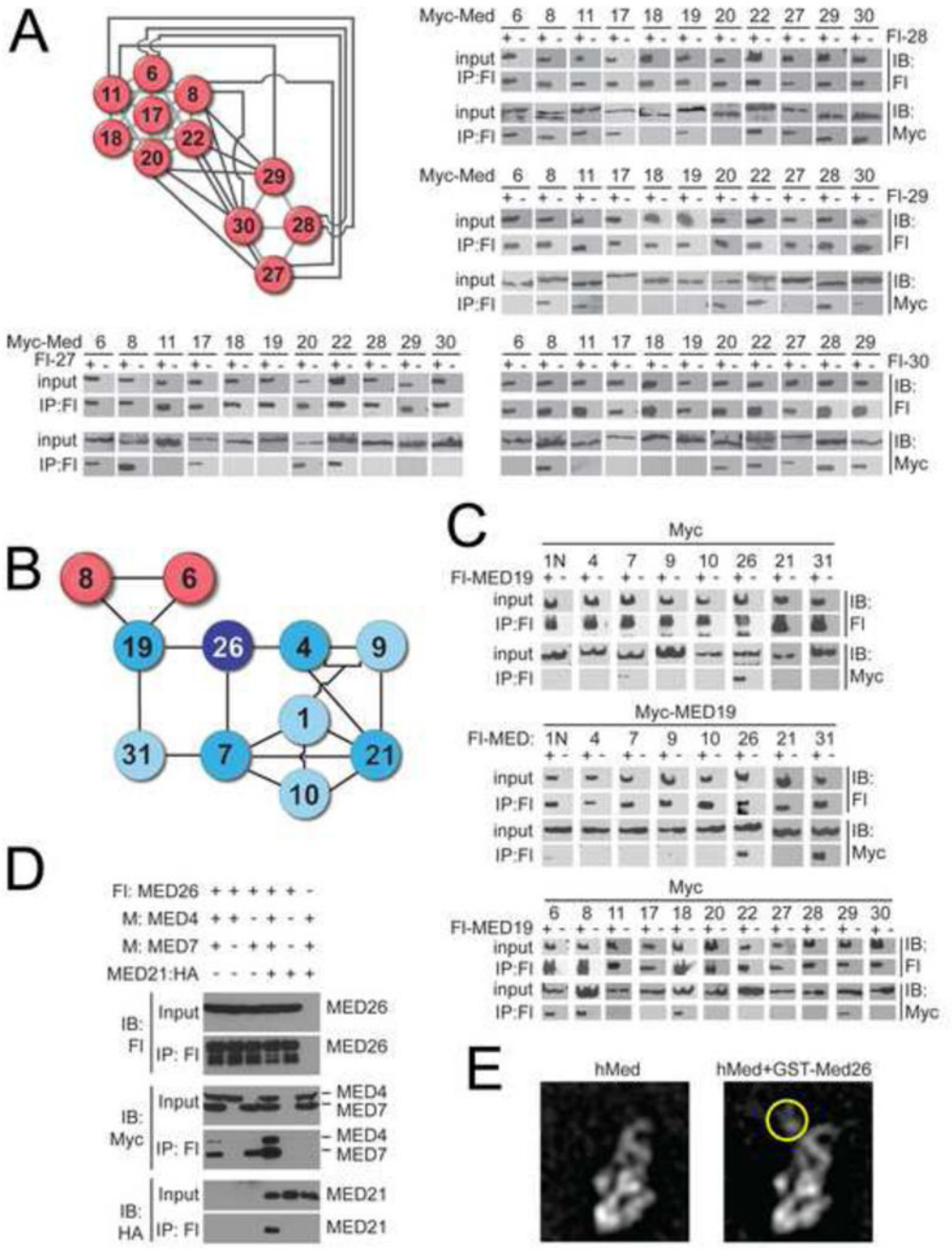

Figure 5. Biochemical analysis of hMED subunit interactions

(A) Metazoan-specific subunits MED27, 28, 29, and 30 interact with human Head module subunits. Immunoblotting of FLAG-immunoprecipitates from lysates (input) from HEK293T cells transiently transfected with the indicated Myc-tagged Mediator (Myc-Med) subunits and FLAG-tagged metazoan-specific subunits MED27, 28, 29, or 30. The diagram summarizes interactions between human Head module subunits detected in these assays and those shown in Fig. S8.

(B) A diagram summarizing interactions between human Head module subunits MED6 and MED8 (red), Middle module subunits (blue), and MED26. Middle module subunits that contact MED26 or are needed to support its incorporation into the middle module are shown in a darker shade of blue.

(C) Human MED19 interacts with Head and Middle module subunits. Immunoblotting of FLAG-immunoprecipitates from lysates (input) from HEK293T cells transiently transfected with FLAG-MED19 and the indicated Myc-tagged Mediator subunits. MED1N, an N-terminal fragment of human MED1 that includes all of the conserved portion of MED1 (residues 1–597) but lacks the nonconserved C-terminal region, was used because it is expressed more highly than its full length counterpart in transiently transfected cells. A similar MED1 N-terminal fragment has been reported previously to be sufficient for Mediator binding (Ge et al., 2008).

(D) MED21 enhances the interaction of MED26 with human MED4 and MED7. Immunoblots (IB) of FLAG-immunoprecipitates (IP) from lysates (input) from HEK293T cells transiently transfected with the indicated combinations of N-terminally FLAG-tagged MED26 (Fl:MED26), Myc-tagged MED4 (Myc:MED4) and MED7 (Myc:MED7), and C-terminally HA-tagged MED21 (MED21:HA).

(E) Localization of MED26 through incubation of hMED with GST-MED26. Scale bar corresponds to 10 nm. See also Figures S4E–F and S5.

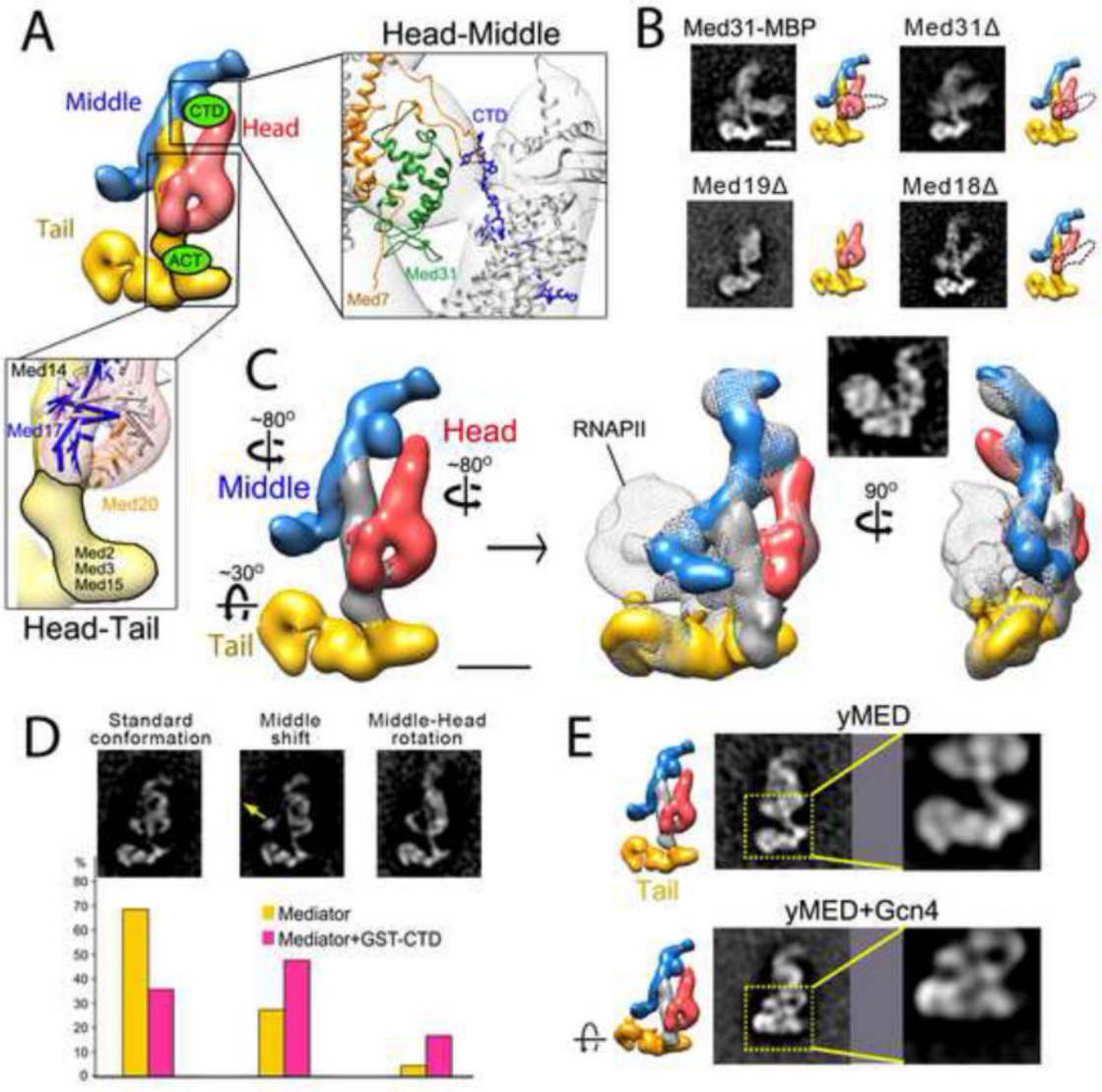

Figure 6. yMED conformational rearrangements and RNAPII interaction

(A) The Head-Middle and Head-Tail module interfaces in yMED appear to be critical for control of yMED conformation. CTD binding at the Head-Middle interface, and targeting of the Head-Tail interface by activators could help explain how yMED conformation is controlled.

(B) Examples of large-scale conformational changes triggered by changes at yMED module interfaces. Tagging or deletion of Med31 destabilizes the contact between the Middle and Head modules (top panels). The Head and Tail modules can interact in the absence of the Middle module, as evidenced in a class average calculated from Med19Δ yMED images (bottom left), but deletion of Med18 (and concomitant loss of Med20) destabilizes the contact between the Head jaws and the Med2-Med3-Med15 connector to the Tail (bottom right). Dashed lines in the schematics represent the altered position of the Head module in corresponding class averages. Scale bar corresponds to 10 nm.

(C) Rigid docking of yMED modules into a published EM map of the yMED-RNAPII-TFIIF holoenzyme (Davis et al., 2002) accounts for all yMED density in the holoenzyme map (shown in mesh) and illustrates the conformational changes required for interaction of yMED with polymerase. A concerted rotation of the Head and Middle modules opens a site for RNAPII binding and the Tail rotates as observed after yMED incubation with Gcn4. Scale bar corresponds to 10 nm.

(D) yMED module rearrangements triggered by incubation with a recombinant GST-CTD. The distribution of yMED particles amongst various conformations (indicated by the bars) shifts considerably after yMED interaction with the CTD, with the Head and Middle modules rotating away from their respective positions in the predominant conformation for yMED alone.

(E) yMED module rearrangements triggered by incubation with a recombinant GST-Gcn4 yeast activator. The activator triggers a change in the conformation of the Med2-Med3-Med15 connector, which results in rotation of the Tail module. See also Figure S6.

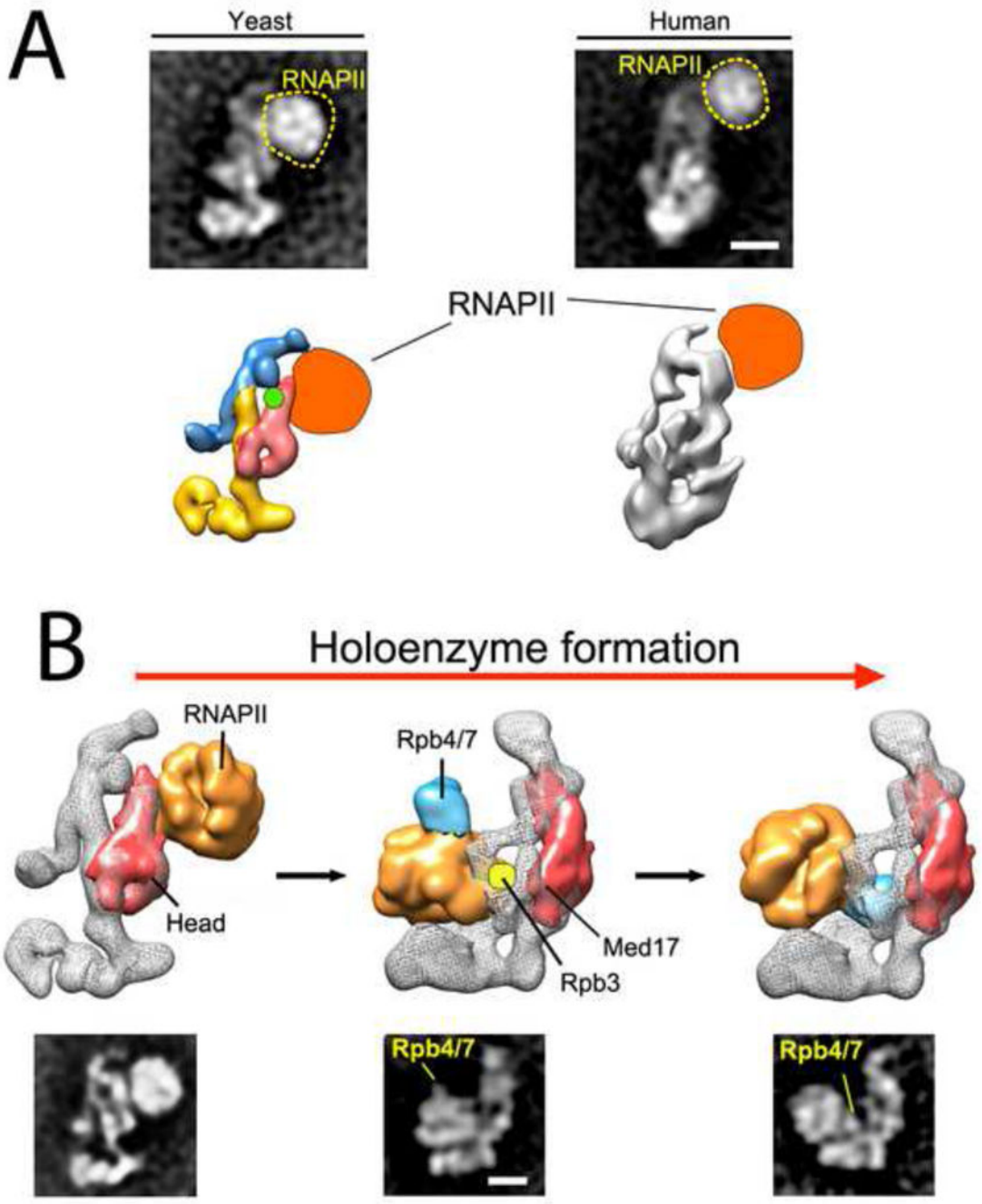

Figure 7. A conserved Mediator mechanism

(A) The initial mode of interaction with RNAPII is conserved between yeast and human Mediators. Scale bar corresponds to 10 nm.

(B) Possible steps in the yMED-RNAPII holoenzyme formation process include migration of RNAPII from its initial CTD-dependent binding site to a “regulation” site generated by yMED conformational changes (Tsai et al., 2013). Once RNAPII reaches the regulation site,

further steps (and almost certainly additional factors) appear to be required to lock the RNAPII orientation and reach full interaction with Mediator.